Size-Dependent Melting of Self-Assembled Indium Nanostructures

M. Dippel,[1] A. Maier,[1] V. Gimple,[1] H. Wider,[1] W. E. Evenson,[2] R. L. Rasera,[3] and G. Schatz[1,*]

[1]*Fachbereich Physik, Universität Konstanz, D-78434 Konstanz, Germany*

[2]*Department of Physics & Astronomy, Brigham Young University, Provo, Utah 84602*

[3]*Department of Physics, University of Maryland, Baltimore County, Baltimore, Maryland 21250*

(Received 5 January 2001; published 13 August 2001)

We have measured the melting temperature of nanoscale indium islands on a WSe_2 substrate using perturbed angular correlations combined with scanning tunneling microscopy. The indium islands are self-assembled nanostructures whose diameter can vary between about 5 and 100 nm, depending on deposition conditions. The melting point decreases due to surface energies as the islands get smaller. This decrease depends on the faceting of the crystalline nanostructures and interactions between the islands and the substrate.

DOI: 10.1103/PhysRevLett.87.095505 PACS numbers: 61.46.+w, 64.70.Dv, 76.80.+y

Production and physical properties of solids with geometrical dimensions in the nanometer range are of great fundamental and technical importance. Two different approaches have been used successfully in the production of nanostructures. First, lithographic and mask techniques permit the creation of periodically arranged nanostructures which extend over large sample areas. A second approach is the growth of nanostructures through self-assembly of deposited atoms or molecules. In this case, structure sizes can be reached which are not limited by wavelengths and mask sizes.

While many techniques are now known to produce nanostructures, it is much more difficult to measure the properties of such small collections of atoms. In our paper, melting of self-assembled nanocrystals of indium in the size range of 5–100 nm produced on a WSe_2 substrate [1] has been studied by combining scanning tunneling microscopy (STM) with perturbed angular correlation (PAC) [2,3]. The size distribution of these nanocrystals is controlled by processing conditions: evaporation rate and substrate temperature. This technique for producing nanostructures works for many different substrates and many deposited materials.

Size-dependent melting of small particles has been studied for many years, both experimentally and theoretically. Transmission electron microscopy (TEM) has been used in a pioneering work by Takagi [4], where a depression of the melting point has been demonstrated when the particle size is in the nanometer range.

A first theoretical description of the melting-point reduction for spherical particles, including surface premelting, was given by Hanszen [5]. This effect was experimentally demonstrated by Wronski [6], and the experiments were further refined by Berman and Curzon [7] for the case of spherical tin and indium particles. The effect of surface premelting for tin nanoparticles was inferred from a measurement of the size-dependent latent heat of fusion using a molecular beam calorimetry technique [8]. This work has recently been extended to particles containing fewer than 500 atoms [9].

TEM has been widely used for the study of the size-dependent melting-point depression. Here specialized thin substrates are needed, and melting is observed by the change in the electron diffraction pattern of a focused electron beam from crystalline to diffuse, where the diffuse pattern comes from the liquid state. X-ray diffraction was also used to study the melting of small particles via either the diffraction intensity or the diffraction peak shape [10,11]. And the field-emission current from individual particles has been used to observe melting of Au and Ag nanoparticles via shape changes [12].

Since TEM is not needed (only STM), the techniques used in this paper are suitable for investigating nanoparticles on a wide variety of interesting substrates and various shapes that may be substrate influenced. The PAC technique is suitable for the study of a wide variety of properties at the nanoscopic level, including crystal symmetry and the melting of nanoparticles (that is exploited here) [2,13,14]. It requires as little as 10^{-4} ML (monolayer) of radioactive probe nuclei, making the technique practical for dilute collections of nanoscale particles. Furthermore, these techniques are temperature insensitive and can be used with the sample in any desired environment.

For the production of our indium nanoparticles, indium was deposited onto single-crystalline WSe_2 substrates with rates from 0.14 to 0.28 nm/s at temperatures of 300 and 193 K [1]. All experimental steps were performed in an ultrahigh-vacuum (UHV) system with a base pressure of 10^{-8} Pa, except that WSe_2 substrates were first cleaved in air and then introduced into the UHV system. The cleanliness of the sample was monitored with Auger electron spectroscopy. Optimizing the deposition rate and substrate temperature, we obtained indium islands with average radii of 5, 19, and 35 nm, and corresponding average heights of 2.3(2), 4.3(2), and 4.4(2) nm. Nanoparticles of these average sizes have about 6×10^3, 1.7×10^5, and 6×10^5

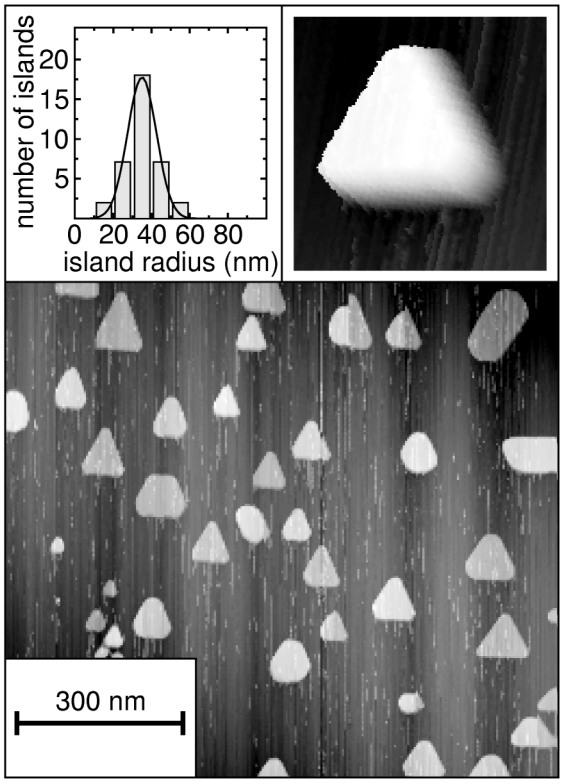

FIG. 1. STM images of indium nanostructures on WSe_2. The islands are faceted (upper right panel) and oriented. A size histogram is also displayed (upper left panel) indicating an average island radius of 35 nm.

atoms, respectively. The size and height of our nanoparticles was determined with *in situ* STM. Figure 1 displays a STM picture of indium nanoparticles with an average radius of 35 nm. The distribution was obtained by inspecting each individual particle and measuring the area, from which an average radius was inferred (upper left panel of Fig. 1). As one can see clearly, the indium nanoparticles grew into triangularlike shapes with well-developed crystal facets (upper right panel of Fig. 1). It is remarkable that, in spite of the weak van der Waals forces on the surface of WSe_2, the substrate imposes registration and orientation on the nanostructures.

For PAC, radioactive ^{111}In probes must be introduced into the nanoparticles. To this end, about 10^{11} ^{111}In atoms are deposited onto the sample after the growth of the nanoparticles. A fraction of the activity is then incorporated via diffusion into the islands, either on rather well-defined bulk lattice sites or on sites in one of the different facets, leading to a variety of local atomic environments. Indium crystallizes in a tetragonal lattice structure, so a nonvanishing electric field gradient is present on regular bulk lattice sites. Upon melting, the crystalline order collapses, and the electric field gradient averages to zero.

^{111}In decays via electron capture to ^{111}Cd ($t_{1/2} = 2.83d$) and then emits a $\gamma\gamma$ cascade which includes an intermediate isomeric $\frac{5}{2}^+$ nuclear state ($t_{1/2} = 85$ ns). This state possesses a nuclear electric-quadrupole moment and therefore interacts with the electric field gradient. This quadrupolar interaction is measured through a perturbation of the $\gamma\gamma$ angular correlation, leading to a time modulation of the $\gamma\gamma$ coincidence rate. Four γ detectors, at angles of 90°, are used to measure the $\gamma\gamma$ coincidences, which for the different detector combinations can be combined into a counting ratio $R(t)$. In our case the $R(t)$ spectrum can be expressed as a superposition of three frequencies, from which the strength, symmetry, and orientation of the electric field gradient can be deduced (for details of the method, see [3]). Figure 2 shows a typical $R(t)$ spectrum together with a Fourier analysis for crystalline indium nanostructures (upper part), clearly exhibiting the expected time modulation and frequency components. For comparison, an $R(t)$ spectrum is shown for molten indium nanostructures; here the oscillatory behavior has disappeared, indicating a vanishing electric field gradient.

With this approach we have studied the fraction of radioactive probes which are exposed to the bulk electric field gradient in the nanostructures as a function of temperature for our three system sizes. The experimental result is summarized in Fig. 3. The measured starting bulk fraction of our probes well below the melting regime diminishes for smaller particle sizes.

We have checked the maximally observable bulk fraction for a 600-ML-thick indium film under identical experimental conditions, yielding 62% ^{111}In probes on well-defined bulk sites. Normalizing to this value, missing fractions of about 25%, 50%, and 75% were still observed for the 35, 19, and 5 nm ensembles, respectively (see Fig. 3). We consider two explanations for the missing fractions, caused either by a cubic environment in the

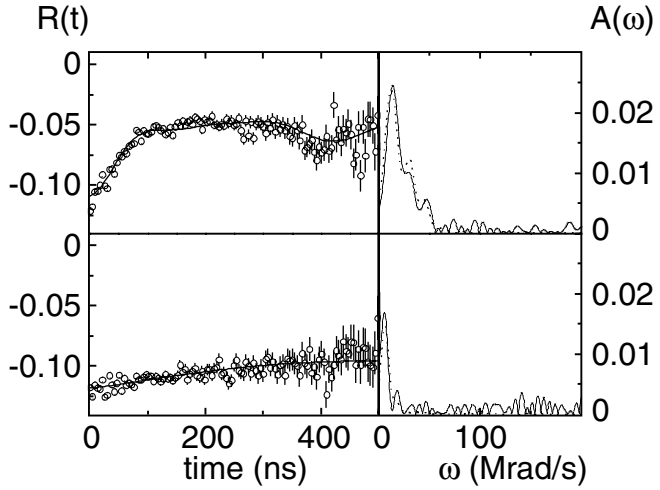

FIG. 2. PAC time spectra together with their Fourier transforms for ^{111}In probes in indium nanostructures with 35 nm average radius. The upper part shows spectra obtained for solid islands ($T = 300$ K); in the lower part the islands are molten ($T = 430$ K).

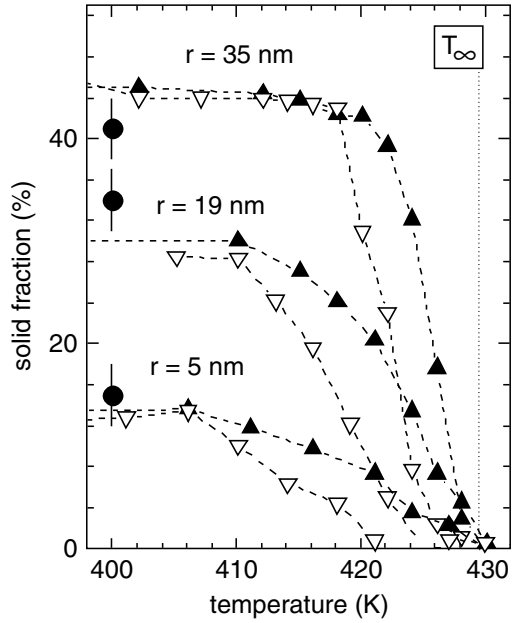

FIG. 3. Fraction of ^{111}In probes exposed to electric field gradients related to the tetragonal crystalline phase of the indium nanostructures as a function of temperature. The closed triangles describe the increasing temperature sequence, and the open triangles describe the cooling sequence. The closed circles at left are the expected starting fractions depending on the surface-volume ratio of the islands (see text). T_∞: melting temperature for bulk indium.

islands resulting in zero electric field gradient or by a fast anisotropy loss due possibly to strong electric field gradients with a broad distribution or to contributions from probes trapped at substrate defects outside the islands. Nevertheless, we emphasize that the source of the missing fraction does not change the interpretation of the results of this paper, since the sum of the observed bulk fraction and the inferred liquid fraction is temperature independent. This clearly indicates that changes in the bulk fraction are due to melting.

Yokozeki and Stein [15] observed a phase transition to fcc structure for particles in a supersonic free jet with radius smaller than 3 nm. Oshima *et al.* [16] also found a sharp transition for indium nanoparticles on a carbon film from bct to fcc below 2.5 nm radius. Rettenberger *et al.* [1] established the bct bulk structure for faceted indium nanostructures with a radius of about 20 nm and a height of 4 nm on WSe_2 by STM studies with atomic resolution. If we assume that 3 nm is the critical size for the bct-to-fcc transition, inspection of the corresponding fraction of particles in our measured size distribution yields no agreement with the observed missing fractions, even considering the relatively small island heights as possibly triggering a transition.

More obvious is an explanation related to the larger surface-to-volume ratio of smaller nanostructures. If we assume a surface layer of about 1.4 nm for which radioactive probes do not contribute to the bulk signal due to strong but topographically varying electric field gradients, a reasonable agreement with the observed bulk fraction can be achieved; this estimate is included in Fig. 3 (closed circles).

The main effect shown in these melting curves is a strong melting-point depression, which is larger for the smaller nanostructures. The melting transition as a function of temperature is rather smooth, due to the size distribution of each of the systems. As an average melting point, we define the temperature at half maximum. During cooling down from the molten into the crystalline state, we also observed a supercooling of about 5 K with respect to the nanoparticle melting point.

For a theoretical understanding of the observed size-dependent melting-point depression, we turn first to existing theories, which are based on the assumption of spherical nanoparticles [6]. Since we are dealing with manifestly nonspherical, triangularlike, highly faceted structures, these theoretical considerations can only be a first-order approach to understanding the basic physical phenomena. Allowing for premelting, i.e., a thin liquid layer on the surface of the spherical particle, the melting-point depression has been well described by [6]

$$T_\infty - T_m = \frac{2T_\infty}{L}\left\{\frac{\sigma_1}{\rho_1(r - t_0)} + \frac{\sigma_2}{r}\left(\frac{1}{\rho_1} - \frac{1}{\rho_2}\right)\right\}, \tag{1}$$

where T_m is the melting temperature at which a solid sphere with radius $r - t_0$ is in equilibrium with a concentric liquid layer of critical thickness t_0, T_∞ is the bulk melting point, L is the latent heat of fusion, σ_1 is the solid-liquid surface tension, σ_2 is the liquid-vapor surface tension, and ρ_1 and ρ_2 are the density of solid and liquid, respectively. For our case we have used the following numerical data: $T_\infty = 156.6\ ^\circ\text{C} = 429.8$ K, $L = 2.834 \times 10^8$ erg/g, $\sigma_1 = 43$ dyn/cm, $\sigma_2 = 569.3$ dyn/cm, $\rho_1 = 7.129$ g/cm^3 (at 156 °C), $\rho_2 = 6.99$ g/cm^3 (at 156 °C), and $t_0 = 2$ nm [17]. These data were taken from Berman and Curzon [7] and the predicted dependence of the relative melting-point depression as a function of nanoparticle radius [Eq. (1)] is shown in Fig. 4 (dashed line). The results for our indium nanostructures are also displayed in Fig. 4 for comparison. The observed melting-point reductions are smaller than expected from theory, at least for our smallest nanostructure sizes. This is not surprising, since in the nanostructures, the binding of atoms in the low-indexed facets at the interface to the liquid layer is higher compared to spherical systems, and it therefore takes more energy to melt the system. In terms of surface tension this can be expressed as a diminishing of the solid-liquid surface tension, which, in view of Eq. (1), would support the tendency of a reduced melting-point depression. Quantitative agreement applying Eq. (1), however, cannot be reached, nor can it be expected, because melting of faceted islands depends strongly on the atomic packing within these facets [18].

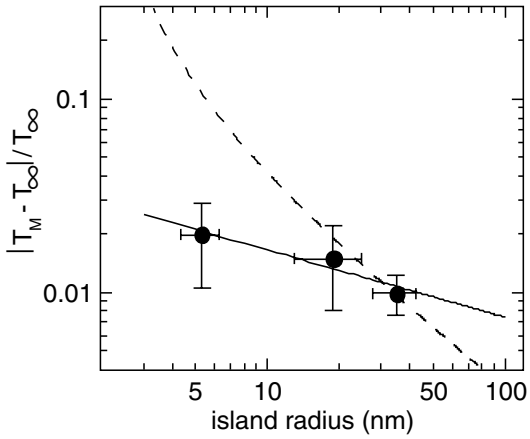

FIG. 4. Relative melting-point depression as a function of indium island radius. The dashed curve represents the theory of melting for spheres including surface premelting [5]. The solid line is a fit to the experimental data yielding an exponent of $\alpha = 0.39(10)$.

Another approach to understanding melting of our nanostructures is finite-size scaling [19], where a relation of the relative melting-point depression to the size of the nanostructures with exponent α is assumed:

$$\frac{|T_m - T_\infty|}{T_\infty} \propto r^{-\alpha}. \tag{2}$$

For first-order phase transitions Landau and Binder [19] carried out by Monte Carlo simulations based on a Potts model and demonstrated that the specific heat maximum should scale with $\alpha = d$, where d is the dimensionality of the system. Log-log axes are used in Fig. 4 in order to show clearly the exponent given by the slope. A fit to the experimental data (solid curve) yields $\alpha = 0.39(10)$. For the thermodynamic theory described above (dashed curve) an exponent $\alpha = 1.0(1)$ is found within the quasilinear range between 10 and 100 nm. Neither case can be explained by the Landau-Binder considerations. Therefore a microscopic approach applying Monte Carlo simulations to a model crystal of nanometer size is needed. Effects of system size and geometry on melting would then be accessible. Such theoretical investigations are in preparation [20].

In summary, we have shown for the first time the melting-point depression for self-assembled, faceted indium nanostructures. The strength of the PAC method has been demonstrated for the study of physical properties on an atomistic length scale. The relatively small melting-point depressions observed in this work are clearly not explained by the classical thermodynamic considerations of melting and premelting. They thus pose a challenge to develop theoretical descriptions for nanostructures with well-defined structural properties.

The authors thank U. Probst and E. Bucher, University of Konstanz, for providing the single-crystal substrates, and J. Boneberg and A. Rettenberger, University of Konstanz, for extremely valuable and inspiring discussions. We are also grateful for continuous and generous support by the Deutsche Forschungsgemeinschaft through the Sonderforschungsbereich 513 at the University of Konstanz. W. E. E. and R. L. R. acknowledge the generous hospitality of Fachbereich Physik at the University of Konstanz, and W. E. E. thanks the German-American Fulbright Commission for support.

*Corresponding author.
Email address: Guenter.Schatz@uni-konstanz.de

[1] A. Rettenberger, P. Bruker, M. Metzler, F. Mugele, Th. W. Matthes, M. Böhmisch, J. Boneberg, K. Friemelt, and P. Leiderer, Surf. Sci. **402–404**, 409 (1998); A. Rettenberger, Ph.D. thesis, University of Konstanz, 1998.
[2] G. Krausch, T. Detzel, H. Bielefeldt, R. Fink, B. Luckscheiter, R. Platzer, U. Wöhrmann, and G. Schatz, Appl. Phys. A **53**, 324 (1991).
[3] G. Schatz and A. Weidinger, *Nuclear Condensed Matter Physics* (Wiley, Chichester, 1996).
[4] M. Takagi, J. Phys. Soc. Jpn. **9**, 359 (1954).
[5] K.-J. Hanszen, Z. Phys. **157**, 523 (1960).
[6] C. R. M. Wronski, Br. J. Appl. Phys. **18**, 1731 (1967).
[7] B. P. Berman and A. E. Curzon, Can. J. Phys. **52**, 923 (1974).
[8] S. L. Lai, J. Y. Guo, V. Petrova, G. Ramanath, and L. H. Allen, Phys. Rev. Lett. **77**, 99 (1996).
[9] T. Bachels, H.-J. Güntherodt, and R. Schäfer, Phys. Rev. Lett. **85**, 1250 (2000).
[10] K. F. Peters, Y.-W. Chung, and J. B. Cohen, Appl. Phys. Lett. **71**, 2391 (1997); K. F. Peters, J. B. Cohen, and Y.-W. Chung, Phys. Rev. B **57**, 13 430 (1998).
[11] Ph. Buffat and J.-P. Borel, Phys. Rev. A **13**, 2287 (1976).
[12] T. Castro, R. Reifenberger, E. Choi, and R. P. Andres, Phys. Rev. B **42**, 8548 (1990).
[13] G. J. Kemerink, F. Pleiter, and G. H. Kruithof, Hyperfine Interact. **35**, 619 (1987).
[14] P. Sinha and G. S. Collins, Nanostruct. Mater. **3**, 217 (1993).
[15] A. Yokozeki and G. Stein, J. Appl. Phys. **49**, 2224 (1978).
[16] Y. Oshima, T. Nangou, H. Hirayama, and K. Takayanagi, Surf. Sci. **476**, 107 (2001).
[17] The values for σ_1 and t_0 were redetermined from Berman and Curzon's published data, Ref. [7], where the melting temperature was inserted into Eq. (1) in °C instead of K for their original analysis.
[18] B. Pluis and A. W. Denier van der Gon, J. W. M. Frenken and J. F. van der Veen, Phys. Rev. Lett. **59**, 2678 (1987).
[19] D. P. Landau and K. Binder, *A Guide to Monte Carlo Simulations in Statistical Physics* (Cambridge University Press, Cambridge, 2000).
[20] H. Knoth and P. Nielaba, University of Konstanz (private communication).